Astron. Astrophys. 347, 442–454 (1999)

ASTRONOMY AND ASTROPHYSICS

# Global spiral modes in star-forming gravitating disks

**Vladimir Korchagin**[1,⋆] **and Christian Theis**[2]

[1] Institute of Physics, Stachki 194, Rostov-on-Don, Russia (vik@rsuss1.rnd.runnet.ru)
[2] Institut für Theoretische Physik und Astrophysik, D-24098 Kiel, Germany (theis@astrophysik.uni-kiel.de)

Received 18 March 1999 / Accepted 11 May 1999

**Abstract.** Using 2D nonlinear simulations, we study the generation and nonlinear evolution of spiral structure in a star-forming multi-component gravitating disk. We confirm in agreement with previous studies the destabilizing role of a cold gaseous component and extend this conclusion for multi-component star-forming disks exchanging mass and momentum between its components. We show that the spiral structure growing on a non-stationary multi-phase background reaches its saturation in a similar manner like the one-component disks. The spiral structure survives even if most of the gas is transformed into stellar remnants of larger velocity dispersion.

**Key words:** hydrodynamics – instabilities – ISM: kinematics and dynamics – galaxies: evolution – galaxies: kinematics and dynamics – galaxies: spiral

## 1. Introduction

The regular spiral arms observed in nearby disk galaxies are a manifestation of global spiral modes developed in galactic disks. Numerous linear and nonlinear studies have demonstrated that self-gravity plays a major role in the generation of global spiral modes (see, e.g. Binney and Tremaine 1987).

Growth of spirals on early stages of galactic evolution, however, occurs on a rapidly changing background. The precursors of present systems look bluer than old galaxies giving evidence for an enhanced star formation rate in early epochs. The colors and irregular structure seen in intermediate red-shifted galaxies suggest that they are a population of galaxies with massive star formation rapidly consuming gas in the galactic disks. These galaxies are the systems where star-formation might considerably change the physics of spiral dynamics.

In this paper we address the question how the evolution of the large-scale spiral perturbations is affected by the processes of mass and momentum exchange in a star forming disk. Kato (1972, 1974) discussed the effects of star-gas mass exchange in a linearly growing spiral mode. Using the WKB-approximation he found, that under some conditions the mass exchange between stars and gas can excite density waves. We extend this study by following the dynamics of the nonlinear hydrodynamical equations for three interacting components: the massive stars, the low mass stars (or stellar remnants) and the gas. We perform a series of 2D multi-phase hydrodynamical simulations of the dynamics of unstable multi-component disks, and compare our results with the morphological properties of spirals, growing in one-component self-gravitating disks. As a particular realization of the mass transformations in star-forming systems we choose the description of Köppen et al. (1995) which is a subset of the more detailed "chemo-dynamical" models developed by Theis et al. (1992), Hensler et al. (1993), Samland (1994) and Samland et al. (1997). Apart from previous papers investigating the interaction network of a multi-component system for spherical (Theis et al. 1992) or axisymmetric galaxies (Samland et al. 1997) we deal here with the evolution of thin, but non-axisymmetric systems. This allows us to study the influence of the interactions between the components on the evolution of spiral structure.

## 2. Basic equations for a three-component star forming disk

The physical processes in star forming galactic disks are too complicated for a detailed analysis from first principles. Among numerous dynamical and interchange processes one has to choose those which have a major influence on the evolution of the system. We perform our analysis using a simplified model which splits the disk into three components regulated by time-dependent mass transformations. We take into account a gas component containing all phases of the interstellar medium, and two stellar components, the massive and the low mass stars. The less massive stars are assumed to have no influence on the interstellar medium, and are simply accumulated as remnants, whereas massive stars are assumed to be responsible for gas heating.

The chain of mass transformations within the model includes spontaneous star formation and ejection of the stellar mass back into the gas phase. For the description of the star formation rate we use the approach developed by Köppen et al. (1995) which is a basic skeleton of the interaction scheme used in chemo-dynamical models (e.g. Theis et al. 1992, Samland et

*Send offprint requests to*: Ch. Theis

⋆ *Present address:* National Astronomical Observatory, Osawa 2-21-1, Mitaka, Tokyo 181, Japan

al. 1997). It describes the spontaneous stellar birth as a power law function of the gas density with an efficiency depending on the temperature of the gas. The latter just has to guarantee that the efficiency drops down with increasing temperature. In this scenario, the chain of mass transformation processes can be described by the following set of equations:

$$\frac{dg}{dt} = -\Psi(g,T) + \eta s/\tau \tag{1}$$

$$\frac{ds}{dt} = \zeta\Psi(g,T) - s/\tau \tag{2}$$

$$\frac{dr}{dt} = (1-\zeta)\Psi(g,T) + (1-\eta)s/\tau \tag{3}$$

where the star formation rate $\Psi(g,T)$ is given by a power law dependence on the gas density $g$ and a function of the gas temperature $T$

$$\Psi(g,T) = C_n f(T) g^n. \tag{4}$$

$s$ denotes the density of massive stars, whereas $r$ corresponds to the low-mass stars and the stellar remnants. The parameters $\zeta$ and $\eta$ determine the fraction of newly born massive stars, and the fraction of gas ejected by massive stars into the ISM, respectively. The parameter $\tau$ corresponds to the mean stellar lifetime of a massive star.

In general, for the determination of the "efficiency" factor $f(T)$ which depends on the gas temperature, one has to integrate the energy balance equation. Köppen et al. (1995) noticed, however, that the model can be simplified, if the time-scales for heating and cooling of the gas are shorter than the characteristic dynamical time-scale of the system. In that case, the effective star formation rate depends only weakly on the exponent $n$ and the efficiency function $f(T)$, and the star formation effectively follows the Schmidt law with the 'true' star formation rate depending quadratically on the gas density. Additionally, due to the self-regulation inherent in this star formation prescription, the effective star formation rate is not strongly affected by substantial variations of $f$ or $C_n$. Therefore, we can restrict our model to the simpler expression

$$\Psi = C_2 g^2. \tag{5}$$

We will use this expression in our analysis.

For the description of the spatial dynamics of the multi-component disk we will use a fluid dynamical approach. In this approach, gas, stars and remnants are considered as three fluids, coupled by nonlinear interchange processes and by the common gravity. While the application of fluid dynamics for the description of the gas is quite natural, it is not obvious that such an approach can be used for the collisionless components of the disk represented by stars and remnants. Kikuchi et al. (1997) analyzed this question and found that the stability properties of disks obtained in fluid approximation are in good qualitative, and to some extent in quantitative agreement with the stability properties of the collisionless models. We will use therefore a fluid approximation in the analysis of perturbations of a multi-component disk. The behavior of our model disk is described by the continuity equations, written for each component, a set of momentum equations, and the Poisson equation. In cylindrical coordinates they are:

$$\frac{D_g\sigma_g}{Dt} = -C_2\sigma_g^2 + \eta\frac{\sigma_s}{\tau} \tag{6}$$

$$\frac{D_s\sigma_s}{Dt} = \zeta C_2\sigma_g^2 - \frac{\sigma_s}{\tau} \tag{7}$$

$$\frac{D_r\sigma_r}{Dt} = (1-\zeta)C_2\sigma_g^2 + (1-\eta)\frac{\sigma_s}{\tau} \tag{8}$$

where $D_{g,s,r}/Dt$ are the corresponding substantial time derivatives written in cylindrical coordinates:

$$\frac{D_{g,s,r}}{Dt} = \frac{\partial}{\partial t} + \frac{1}{r}\frac{\partial}{\partial r}ru_{g,s,r} + \frac{1}{r}\frac{\partial}{\partial\phi}v_{g,s,r} \tag{9}$$

Using Eqs. (6)–(8) and definition (9) the momentum equations can be written as

$$\sigma_g\frac{D\mathbf{v_g}}{Dt} + \nabla P_g + \sigma_g\nabla\Big(\Phi + \Phi_H + \Phi_B\Big) = -C_2\sigma_g^2\mathbf{v_g} + \eta\frac{\sigma_s}{\tau}\mathbf{v_s} \tag{10}$$

$$\sigma_s\frac{D\mathbf{v_s}}{Dt} + \nabla P_s + \sigma_s\nabla\Big(\Phi + \Phi_H + \Phi_B\Big) = \zeta C_2\sigma_g^2\mathbf{v_g} - \frac{\sigma_s}{\tau}\mathbf{v_s} \tag{11}$$

$$\sigma_r\frac{D\mathbf{v_r}}{Dt} + \nabla P_r + \sigma_r\nabla\Big(\Phi + \Phi_H + \Phi_B\Big) = (1-\zeta)C_2\sigma_g^2\mathbf{v_g} + (1-\eta)\frac{\sigma_s}{\tau}\mathbf{v_s} \tag{12}$$

Here $\sigma_{g,s,r}$ are the surface densities, and $u_{g,s,r}$ and $v_{g,s,r}$ are the radial and azimuthal components of the velocities $\mathbf{v_{g,s,r}}$ of gas, stars and remnants in the disk.

Without the exchange processes, i.e. when the right-hand sides of the Eqs. (10)–(12) are zero, the dynamics of these quantities is determined by the partial "pressures" of the components $P_{g,s,r}$, the self-gravity of the disk $\Phi$ and the external gravity of the halo and bulge, $\Phi_H$ and $\Phi_B$. Mass transformations between the components give an additional factor for the momentum balance and have to be taken explicitly into account in the numerical simulations.

The gravitational potential $\Phi$ is determined by the overall density of all components, and can be written in the form of a Poisson integral as

$$\Phi = -G\int_{R_{\rm in}}^{R_{\rm out}}(\sigma_g(r',\phi') + \sigma_s(r',\phi') + \sigma_r(r',\phi'))r'dr' \cdot\int_0^{2\pi}\frac{d\phi'}{\sqrt{r^2+r'^2-2rr'\cos(\phi-\phi')}} \tag{13}$$

The equation of state closes the system of Eqs. (6)–(12). Throughout the simulations we use a polytropic equation of state applied to all three components:

$$P_{g,s,r} = K_{g,s,r}\sigma_{g,s,r}^{\gamma_{g,s,r}} \tag{14}$$

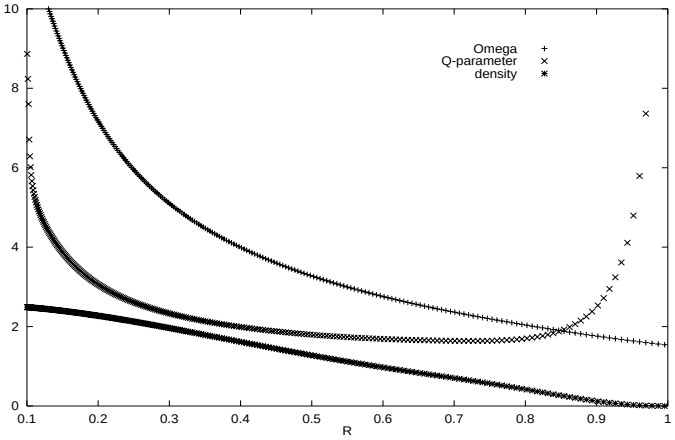


**Fig. 1.** Radial dependence of the angular velocity $\Omega$, the Toomre-parameter $Q$, and the equilibrium density $\sigma$ for a purely stellar disk ($\gamma = 2$) with exponential surface density distribution.

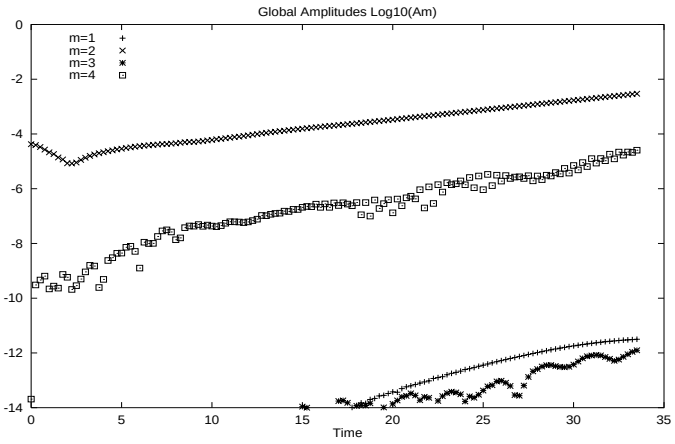


**Fig. 2.** Temporal evolution of the global amplitudes $\log(A_m)$ ($m = 1, 2, 3, 4$) for a purely stellar disk ($\gamma = 2$) with exponential surface density distribution.

Eqs. (6)-(14) are used for the analysis described in the subsequent sections.

In our simulations we will use a "galactic" system of units in which $R = 20$kpc, $M = 10^{11} M_\odot$ and the gravitational constant $G$ is unity. With this choice we have a unit of time equal to $1.33 \times 10^8$ yr, and a unit of velocity equal to $147\,\mathrm{km\,s^{-1}}$.

## 3. Axisymmetric distributions

We assume that all three components have axisymmetric flat rotation curves in the outer regions of the disk. The quasi-stationary equilibrium rotation is jointly supported by the gravity of the halo and bulge, the self-gravity of the disk and the pressure gradient:

$$r\Omega_i^2(r) = \frac{\partial}{\partial r}(\Phi_H + \Phi_B + \Phi_{0i} + P_{0i}) \tag{15}$$

Here $\Omega_i(r)$ is the angular velocity in the disk, $\Phi_{0i}$ is the axisymmetric self-gravitating potential, and $P_{0i}$ are the partial pressures of the components corresponding to their unperturbed density distributions.

In our simulations, we consider two types of the equilibrium rotation curves and surface density distributions. In the first experiment, we choose the exponentially decreasing surface density of the disk with density distributions of all three components given by the expression

$$\sigma_{g,s,r}(r) = M_{g,s,r} \cdot \exp\Big(-d_1 \cdot \sqrt{d_2 + d_3 \cdot r^2}\Big) \cdot \Big[1 - \exp\Big(-\frac{(r - R_{\rm out})^2}{r_s^2}\Big)\Big]^4 \tag{16}$$

with the normalization constants $M_{g,s,r}$ which are the masses of the gaseous, stellar and remnant component. The halo-bulge potential determining the rotational curve (16) is similar to that used by Vauterin and Dejonghe (1996). Namely, we assume that the external potential has the form

$$\frac{\partial \Phi_H}{\partial r} + \frac{\partial \Phi_B}{\partial r} = M_H \frac{r}{(r^2 + R_H^2)^{\frac{3}{2}}} + M_B \frac{r}{(r^2 + R_B^2)^{\frac{3}{2}}}. \tag{17}$$

In a thin disk with sharp boundaries the potential diverges at its edges. To study to what extent the sharp cut-off in an unperturbed density distribution influences the results, we performed, additionally, experiments using a Gaussian-type density distribution vanishing at both boundaries:

$$\sigma_{g,s,r}(r) = M_{g,s,r}\Big[1 - \exp\Big(-\frac{(r - R_{\rm in})^2}{r_s^2}\Big)\Big]^4 \cdot \Big[1 - \exp\Big(-\frac{(r - R_{\rm out})^2}{r_s^2}\Big)\Big]^4 \exp\Big(-\frac{(r - R_0)^2}{\omega}\Big) \tag{18}$$

In this case the disk is kept in centrifugal equilibrium by an alternative bulge/halo distribution resulting in a radial acceleration of the form

$$\frac{\partial \Phi_H}{\partial r} + \frac{\partial \Phi_B}{\partial r} = v_\infty^2 \frac{r}{r^2 + R_H^2} + M_B \frac{r}{(r^2 + R_B^2)^{\frac{3}{2}}}. \tag{19}$$

Both halo and bulge potentials, described by the Eqs. (17) and (19) dictate the "flat" rotation in the outer region of the disk. The parameters $R_H$ and $R_B$ in Eqs. (17) and (19) determine the spatial scales of the halo and bulge density distributions, $v_\infty$ gives the asymptotic value of the rotational velocity, and $M_H$ and $M_B$ determine the masses of the halo and the central bulge.

## 4. Parameters of the model

We consider the dynamics of the disk by setting the radius of the innermost boundary cell to $R_{\rm in} = 0.1$, and the radius of the outer boundary cell to $R_{\rm out} = 1$.

The group of parameters $\tau, \zeta, \eta$ and $C_2$ in the right-hand side of the continuity Eqs. (6)-(8) govern the interchange processes between the components. Following Köppen et al. (1995) we choose the mean stellar lifetime $\tau = 10\,$Myr, or in our units $\tau = 0.075$. The mass fraction $\zeta$ of the newly formed massive stars was set to 0.12. This value corresponds to a Salpeter-IMF ranging from 0.1 $M_\odot$ to 100 $M_\odot$ and a lower mass limit of

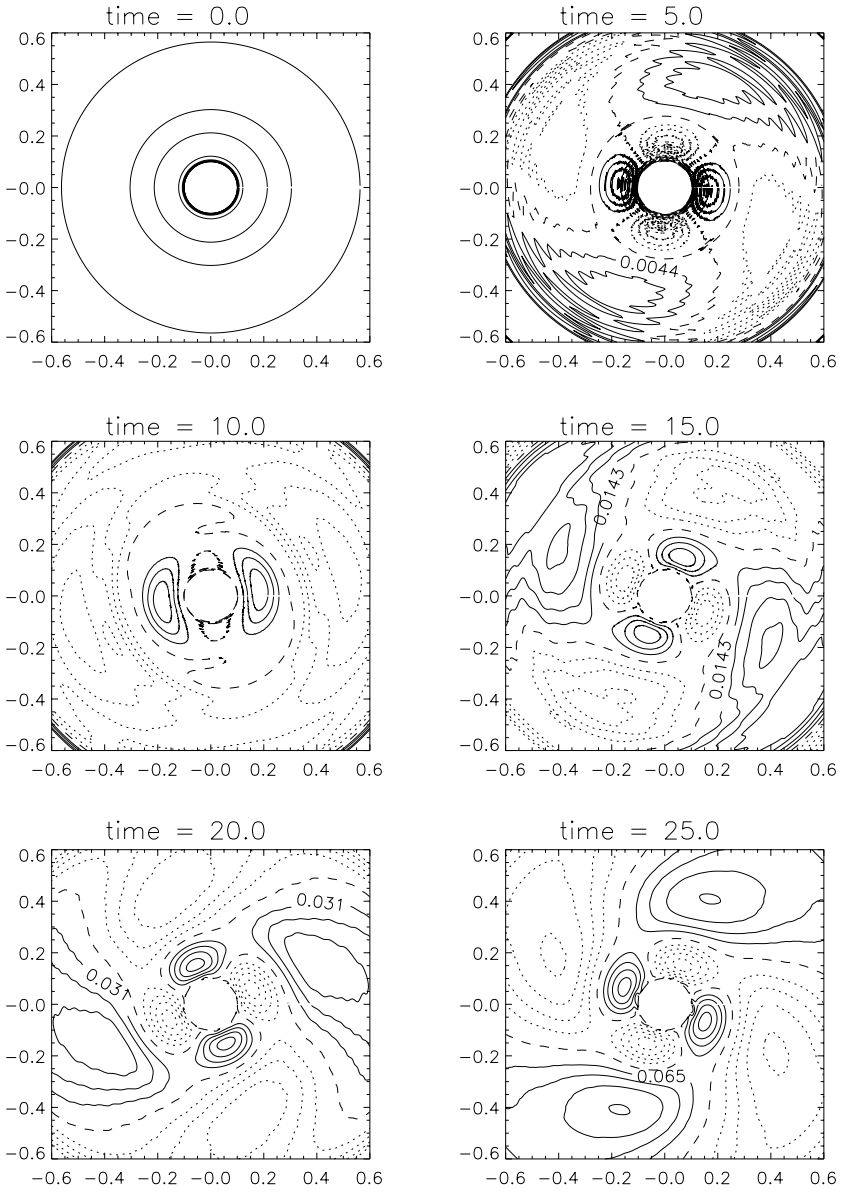


**Fig. 3.** Contour maps of the radial velocity (in $\mathrm{km\,s^{-1}}$) of a purely stellar disk ($\gamma = 2$) with an exponential surface density distribution at different times: $t = 0$ (*upper left*), $t = 5$ (*upper right*), $t = 10, 15, 20, 25$. The contours give 30%, 50%, 70% and 90% of the maximum velocity in each diagram. The dotted lines correspond to negative velocities, whereas the solid lines give positive velocities. The zero-velocity contour is shown with a dashed line.

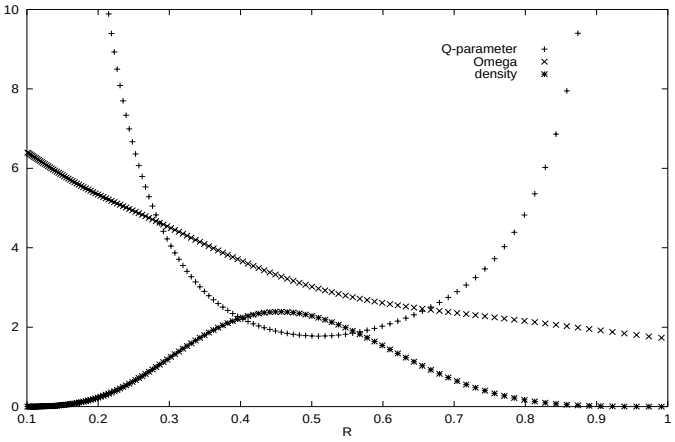


**Fig. 4.** Radial dependence of the angular velocity $\Omega$, the Toomre-parameter $Q$, and the equilibrium density $\sigma$ for a purely stellar disk ($\gamma = 2$) with the Gaussian surface density distribution.

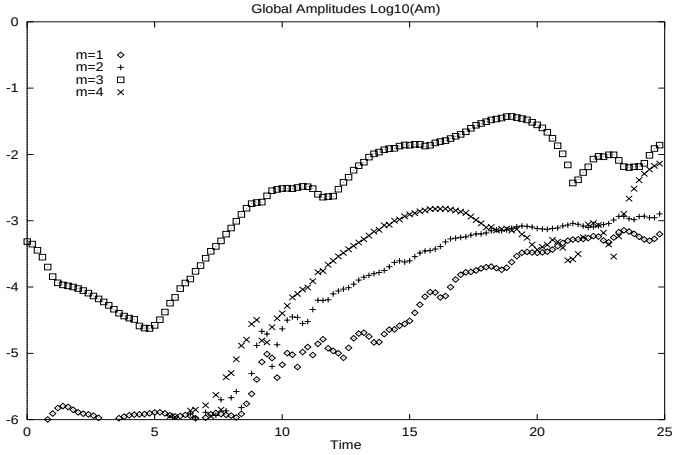


**Fig. 5.** Temporal evolution of the global amplitudes $\log(A_m)$ ($m = 1, 2, 3, 4$) for a purely stellar disk ($\gamma = 2$) with the Gaussian surface density profile.

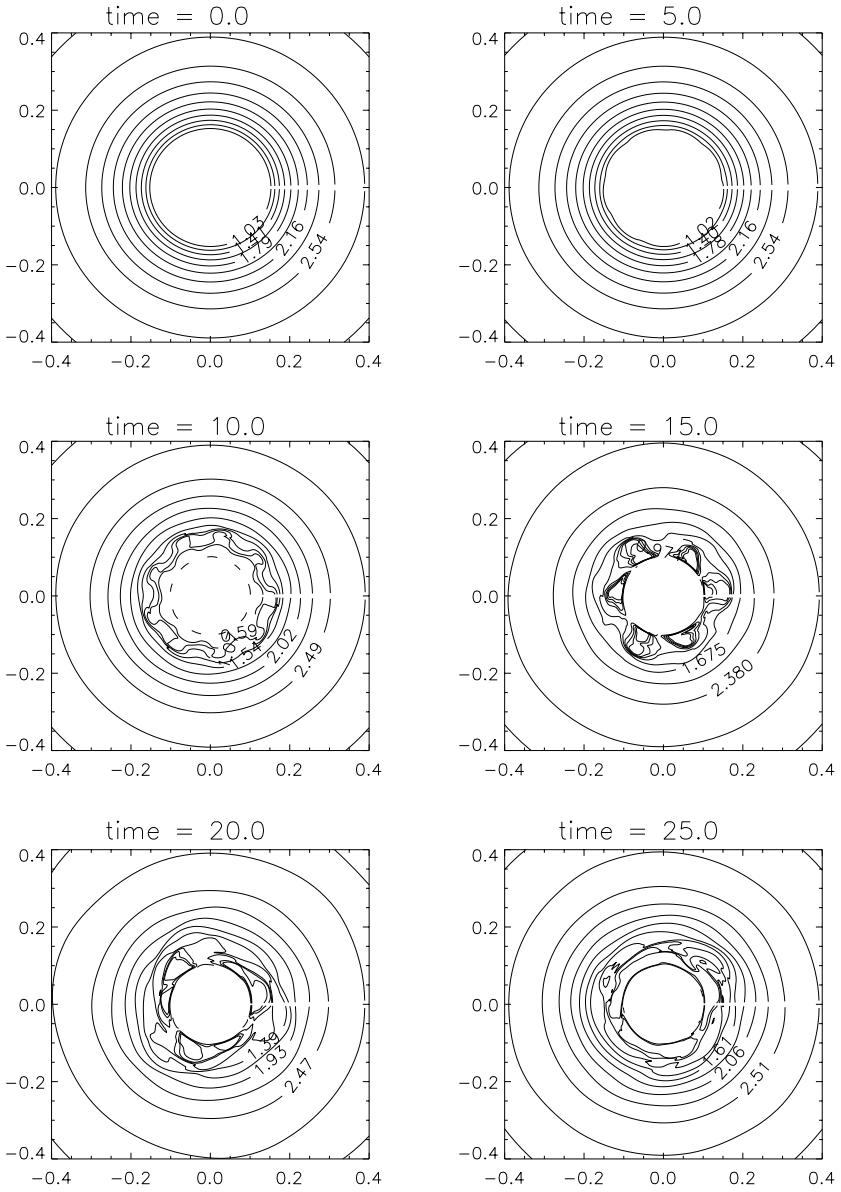


**Fig. 6.** Contour maps of the logarithmic surface density ($\mathrm{M}_\odot/\mathrm{pc}^2$) for a purely stellar Gaussian disk ($\gamma = 2$) at different times: $t = 0$ (*upper left*), $t = 5$ (*upper right*),

massive stars of 10 $M_\odot$. The fraction $\eta$ of mass ejected by massive stars back to the interstellar medium was taken to be 0.9.

The parameter $C_2$ was set to 0.1. With this choice, the maximum star-formation rate in our model is 0.025, or $\approx 18 M_\odot/\mathrm{yr}$ if the initial mass of the gaseous disk is equal to 0.5 in our units. This value of the star-formation rate is close to the maximum star-formation rate obtained in chemo-dynamical models for the evolution of disk galaxies (Samland 1994).

We have assumed that the gas component of the disk is mainly composed of mono-atomic hydrogen with a volume polytropic index $\gamma_g = 1.67$. The polytropic constant for the collisionless stellar component and the remnants was set to 2.0. There are a few arguments in favor of this choice. Marochnik (1966) found that in a rigidly rotating disk the dynamics of perturbations can be described by introducing the polytropic equation of state with $\gamma_s = 2$. This value is consistent with the empirical "square root law" found by Bottema (1993) in his studies of nearby spiral galaxies. He found, that the surface density distribution of stars, and their radial velocity dispersion are related as $c_s \propto \sqrt{\sigma(r)}$. It is easy to see, that such a "square root law" requires the value of the effective polytropic index to be $\gamma_s = 2$. Kikuchi et al. (1997) made a detailed comparison of the linear stability properties of the exact collisionless models investigated by Vauterin & Dejonghe (1996) with the stability properties of this model studied in a fluid dynamical approach. They found a full qualitative agreement between these two approaches. Thus, a fluid dynamical approximation can be used for the analysis of the multi-component disks. The constant $K_g$ was set to be 0.04 resulting in a Toomre-stable disk (for details, see Sect. 6). The values $K_s$ and $K_r$ have been set to twice this value. This choice corresponds to a larger "sound" velocity of the stars, by this mimicking as well the dynamical heating of disk stars as the lack of dissipation in the stellar component.

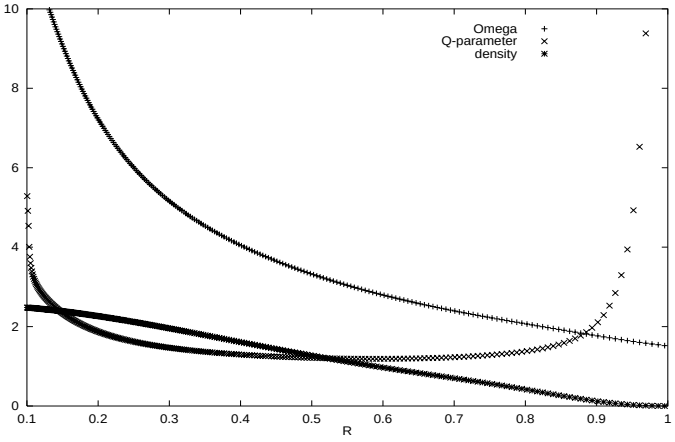


**Fig. 7.** Radial dependence of the angular velocity $\Omega$, density distribution and the Toomre-parameter $Q$ for the gaseous component in a multi-component disk with the exponential surface density distribution.

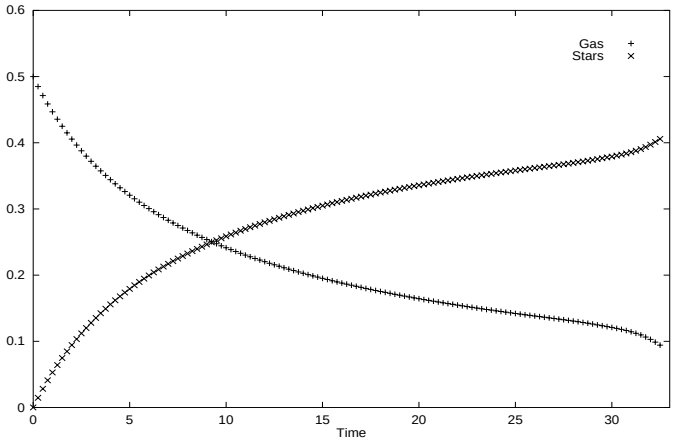


**Fig. 8.** Temporal evolution of the masses of gaseous and the stellar component in a multi-component disk with an exponential density distribution.

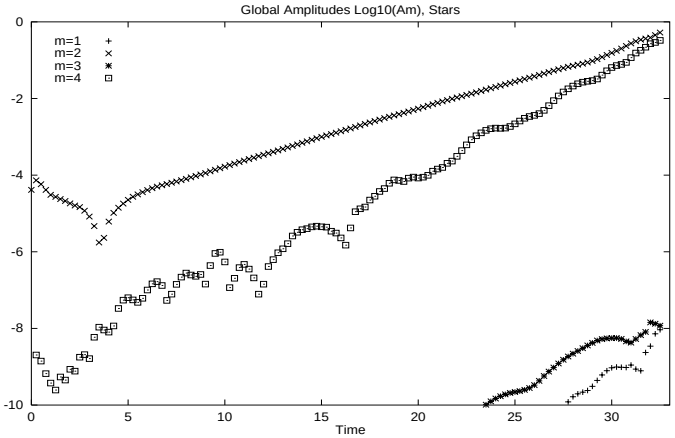


**Fig. 9.** Temporal evolution of the global amplitudes $\log(A_m)$ ($m = 1, 2, 3, 4$) for stellar component of the multi-phase disk with an exponential density distribution.

All parameters including those which are not discussed in this section are listed in the tables in the appendix.

## 5. The code

For solving the multi-component hydrodynamical Eqs. (6)–(12) we use a second order Van Leer advection scheme as implemented by Stone & Norman (1992) in a general purpose fluid dynamics code, called ZEUS-2D. This code was designed for modeling astrophysical systems in two spatial dimensions, and can be used for simulations of a wide variety of astrophysical processes. The ZEUS-2D code uses sufficiently accurate hydrodynamical algorithms which allow to add complex physical effects in a self-consistent fashion. This code provides therefore a good basis for the implementation of the nonlinear mass transfer processes into the multi-phase hydrodynamics.

The Eulerian codes with the Van Leer advection scheme were successfully used for the investigation of the stability of self-gravitating disks (Laughlin & Różyczka 1996, Laughlin et al. 1997, 1998). The main difference between the "standard" ZEUS-type codes and our one is the introduction of mass and momentum interchange processes between different components. These processes can be computed at the first sub-step of the ZEUS-type code which makes a generalization of the ZEUS-type code straightforward.

Briefly, the code solves the hydrodynamical equations using equally spaced azimuthal zones and logarithmically spaced radial zones. For the simulations discussed here we mainly employed a grid with $256 \times 256$ cells. To advance the solutions due to interchange processes given by the right-hand sides of the Eqs. (6)-(8) we used the fifth order Cash-Karp Runge-Kutta routine with the time step limitation imposed by the Courant-Friedrichs-Levy criterion and the values of the parameters $\tau$ and $C_2$ in mass and momentum interchange processes. The Poisson equation is solved by applying the 2D Fourier convolution theorem in polar coordinates.

## 6. Global instability of a one-component disk

In order to understand the influence of mass and momentum exchange processes on the evolution of global modes in a self-gravitating disk we performed simulations of the dynamics of a one-component stellar disk. The equilibrium stellar disk was chosen to have the surface density distribution (16). The parameter $M_s$ for the stellar disk was selected so that the disk's total mass is equal to 0.5.

Fig. 1 shows the equilibrium properties of the stellar disk used in the analysis. The Toomre $Q$-parameter, which is defined for the stellar disk as $Q \equiv c_s\kappa/3.36G\sigma$, has a profile typical for the density distribution given by Eq. (16). The $Q$-profile rises towards the boundaries of the disk, with a minimum value of 1.64 at radius 0.73 indicating a globally stable disk with respect to Toomre's stability criterion $Q > 1$.

The one-component stellar disk was perturbed with an $m-$armed perturbation of the form

$$\sigma_s(r,\phi) \;=\; \sigma_s(r) \cdot [1 + 0.001\cos(m\phi)] \cdot \qquad (20)$$

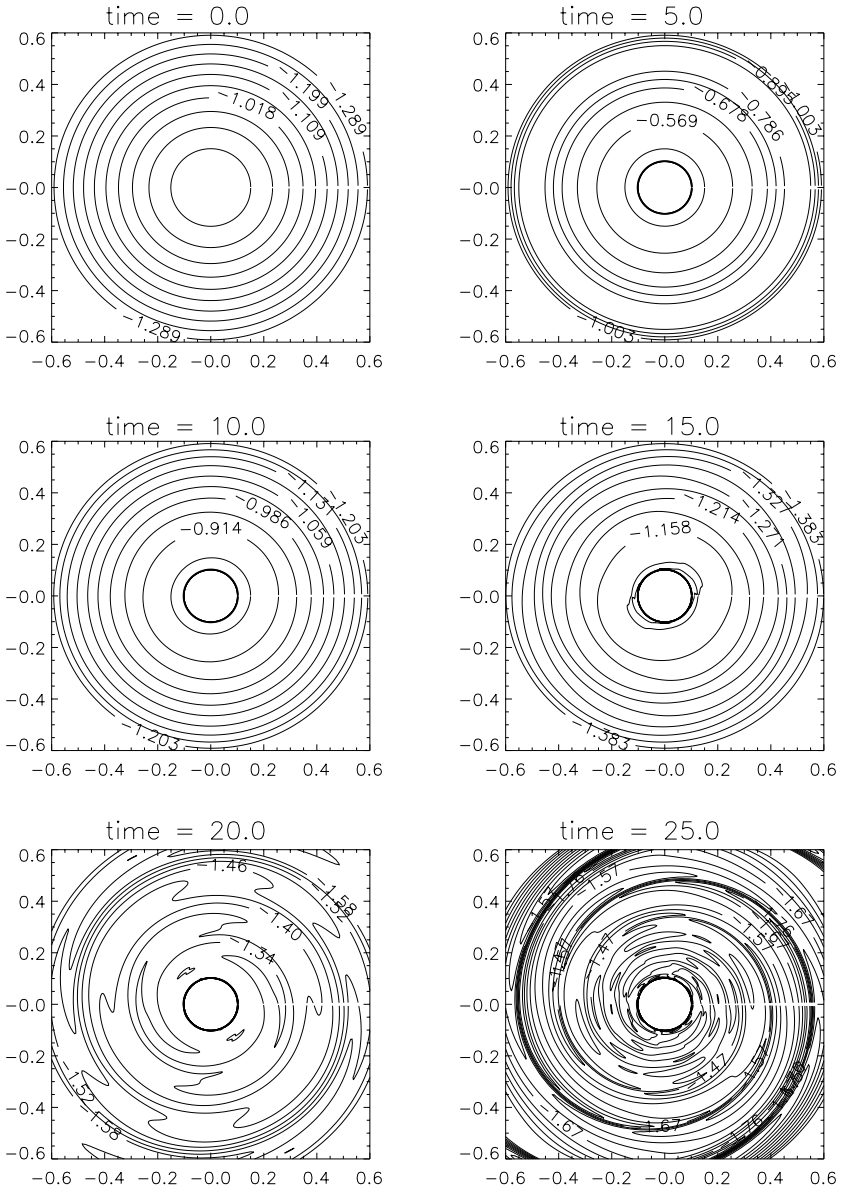


**Fig. 10.** Contour maps of the logarithmic surface density ($\mathrm{M}_\odot/\mathrm{pc}^2$) of the stars for the multi-phase exponential disk at different times: $t = 0$ (*upper left*), $t = 5$ (*upper right*), $t = 10, 15, 20, 25$. The contours are logarithmic-equally spaced. The equilibrium model is perturbed by an $m = 2$-mode.

$$\cdot\Big[1-\exp\Big(-\frac{(r-R_{\rm in})^2}{r_s^2}\Big)\Big]^5\cdot$$
$$\Big[1-\exp\Big(-\frac{(r-R_{\rm out})^2}{r_s^2}\Big)\Big]^5.$$

We chose $m = 2$ and $m = 3$ perturbations in studying the stability properties of our models.

Fig. 2 plots the development of the global amplitudes for $m = 1, 2, 3$, and $m = 4$ spiral modes in a stellar disk seeded by an $m = 2$ perturbation of the form (20). The global amplitudes defined by the expression

$$A_m = \frac{|\int_0^{2\pi}\int_{R_{\rm in}}^{R_{\rm out}}\sigma(r,\phi)dre^{-im\phi}d\phi|}{\int_0^{2\pi}\int_{R_{\rm in}}^{R_{\rm out}}\sigma(r,\phi)drd\phi} \qquad (21)$$

illustrate the overall dynamics of the particular global mode.

Fig. 2 shows a slow exponential growth of the $m = 2$ mode. The $m = 1$, $m = 3$ and $m = 4$ armed spirals grow, too, but due to the initial conditions, the $m = 2$ global mode outstrips the other competitor modes during the whole computation. However, even at the late stages of evolution the amplitude of spiral perturbations is less then half percent, and the spiral pattern does not emerge from the background. The slow development of the perturbation is best seen on the sequence of the snapshots shown in Fig. 3 illustrating the contour plots of the perturbed radial velocity. (The orbital periods at the inner and outer boundary are 0.59 and 4.16, respectively.)

Similar behavior was observed in the stellar disk with the Gaussian surface density distribution (18) and the rotation curve (19). Fig. 4 shows the equilibrium properties of this disk which is rather stable with a minimum value of Toomre's Q-parameter equal to 1.78 at a disk radius of $R = 0.5$.

This disk was seeded with a three-armed perturbation of the form (20). As it is seen from Fig. 5, the disk develops a set of slowly growing modes. The behavior of the global amplitudes

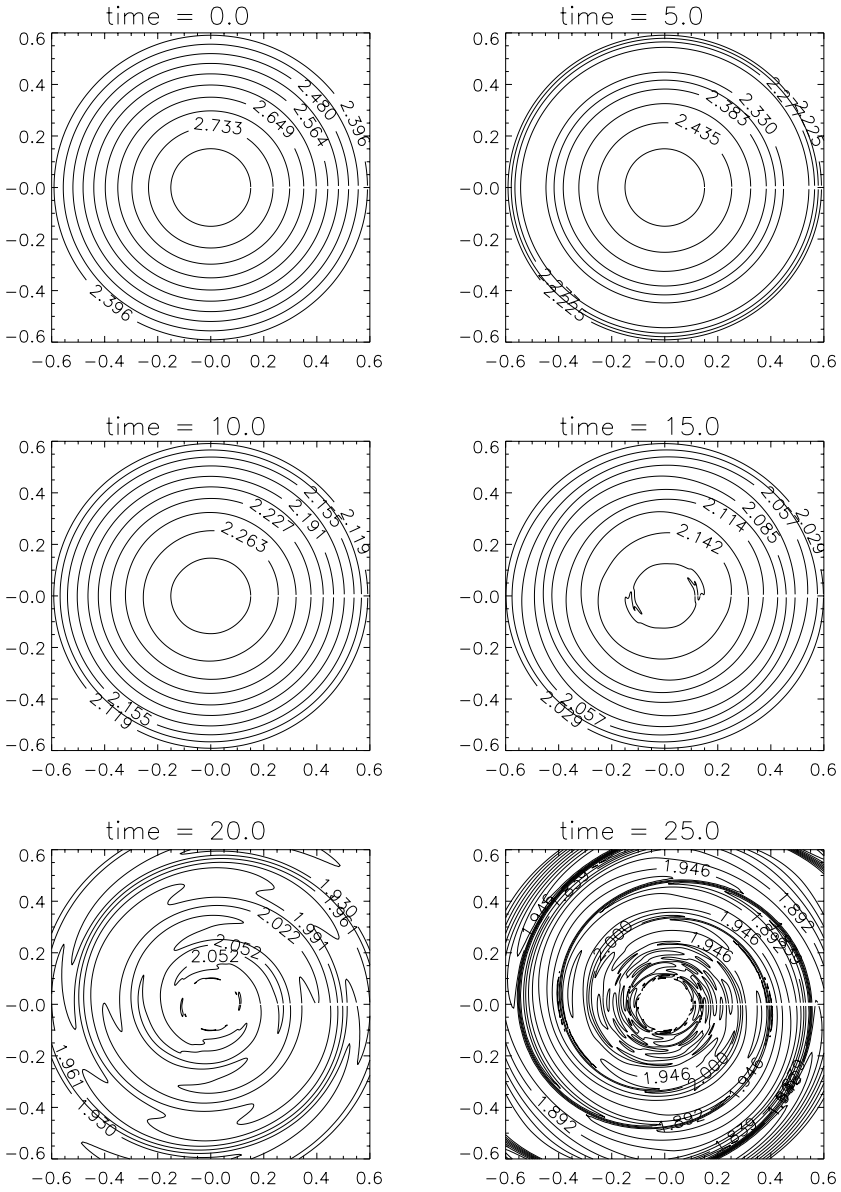


**Fig. 11.** Contour maps of the logarithmic surface density ($\mathrm{M}_\odot/\mathrm{pc}^2$) of the gas for the multi-phase exponential disk at different times: $t = 0$ (*upper left*), $t = 5$ (*upper right*), $t = 10, 15, 20, 25$. The contours are logarithmic-equally spaced. The equilibrium model is perturbed by an $m = 2$-mode.

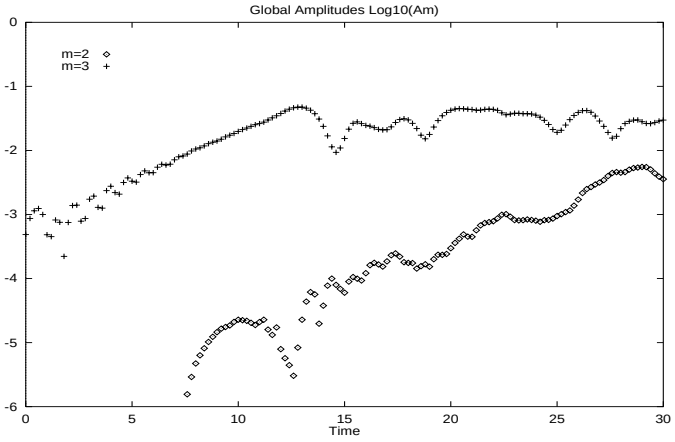


**Fig. 12.** Temporal evolution of the global amplitudes $\log(A_m)$ of the $m = 2$ and $m = 3$ modes for the stellar component of the multi-phase disk with the Gaussian density profile.

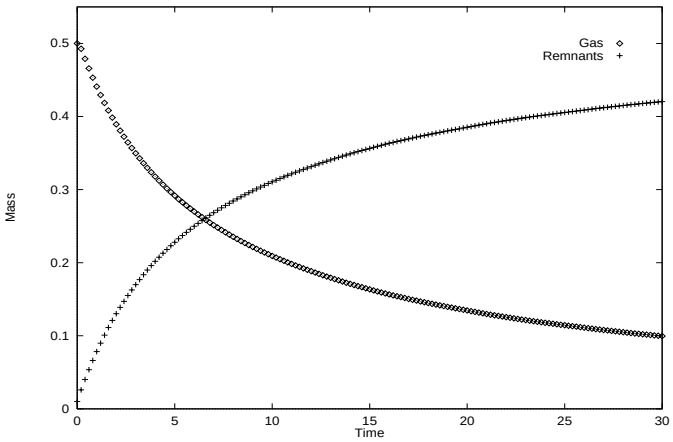


**Fig. 13.** Mass transformations between the gaseous and stellar components in the multi-phase disk with the Gaussian density distribution.

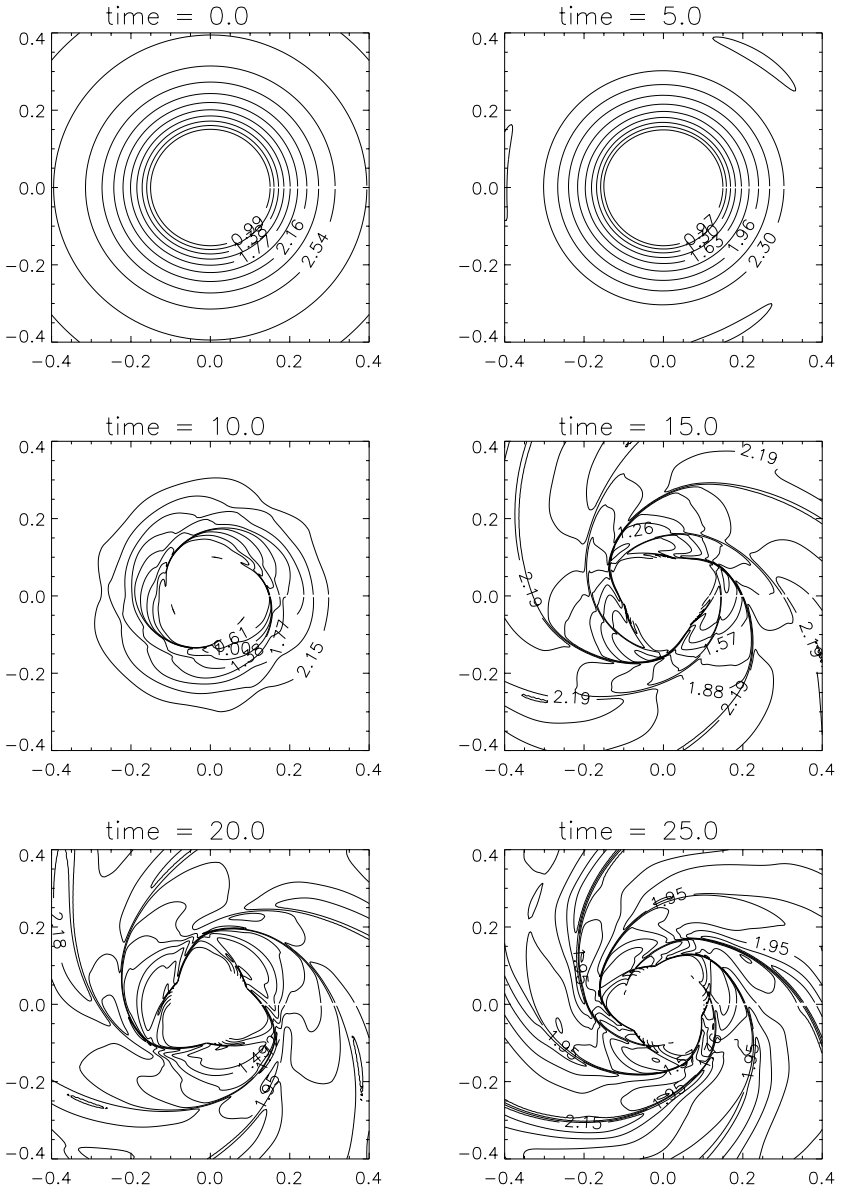


**Fig. 14.** Contour maps of the logarithmic surface density ($\mathrm{M}_\odot/\mathrm{pc}^2$) of the gas for the multi-phase Gaussian disk at different times: $t = 0$ (*upper left*), $t = 5$ (*upper right*), $t = 10, 15, 20, 25$. The contours are logarithmic-equally spaced. The equilibrium model is perturbed by an $m = 3$-mode.

is somewhat similar to the previous case. (The orbital periods at the inner and outer boundary amount here to 0.97 and 3.65, respectively.) The $m = 3$ spiral mode has higher amplitude compared to the other competitors, and has a tendency to be saturated at the level $\log(A_3) \approx -2$. The perturbation, however, does not have any properties of a regular spiral pattern (Fig. 6). Even at the late stages of the evolution the contours remain quite patchy, and do not resemble the regular spiral pattern.

In the next section we will discuss how the morphological properties of the global modes are affected by the *change* of the equation of state which is a necessary consequence of a phase transformation in a star-forming disk.

## 7. Global modes in a multi-component disk

To compare the behavior of a multi-component disk with the dynamics of a corresponding one-component system, the surface densities of all phases were initially distributed in accordance with Eqs. (16) or (18). In both cases we choose the initial mass of the gaseous component equal to the mass of the one-component system. Masses of the "admixture", i.e. stars and remnants, were initially set to 0.01 each which is about two percent of the initial mass of the gaseous component. All components were set at the beginning into centrifugal equilibrium, with the circular rotation supported by the pressure gradients of the components, the total gravitational field of the three components and the gravity of the external halo. Fig. 7 shows the rotation curve and the epicycle frequency of the gaseous component for the initial exponential surface density distributions. The rotation curve of the gaseous component is very similar to the equilibrium profiles of the stellar disk discussed in the previous section (Fig. 1). However, the gaseous component is less stable compared to the purely stellar disk, and the broad trough of Toomre's Q-parameter lies below the corresponding Q-distribution of the stellar disk.

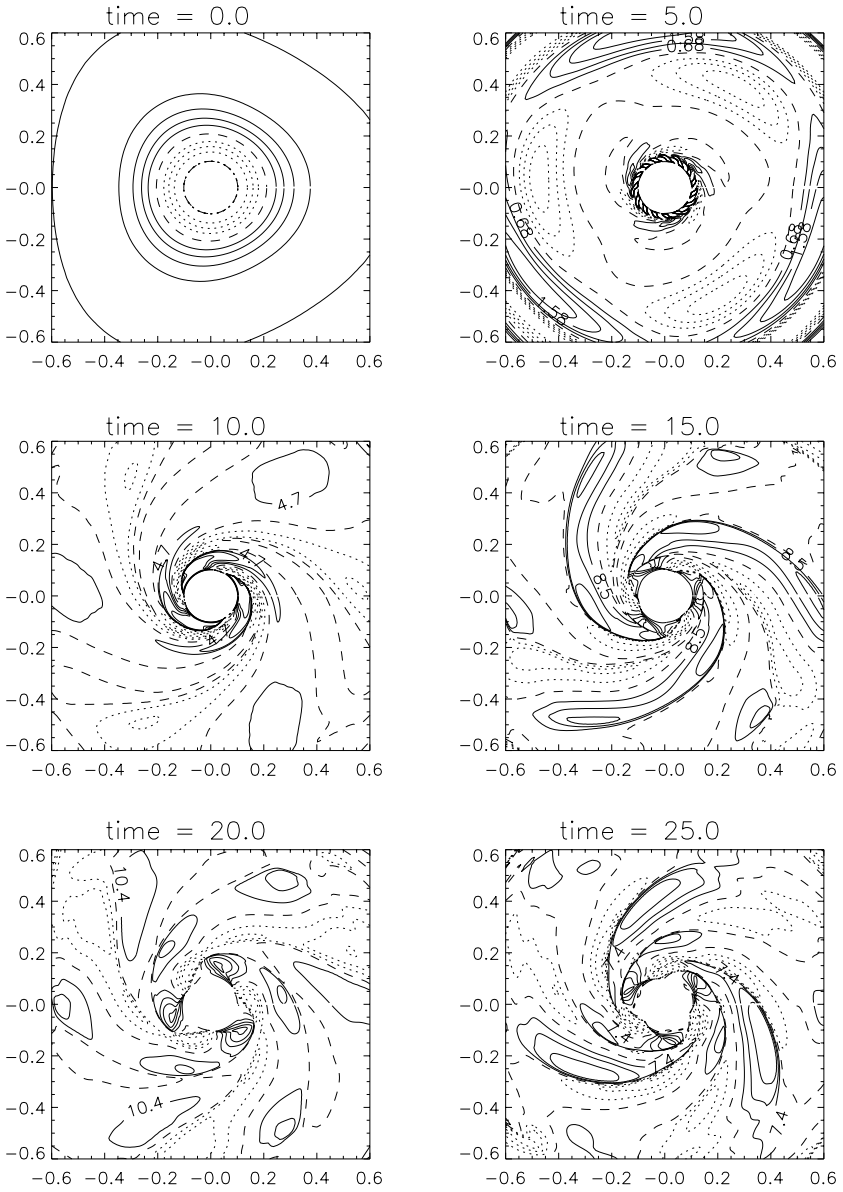


**Fig. 15.** Contour maps of the radial velocity (in $\mathrm{k\,ms^{-1}}$) of the gaseous component in the Gaussian disk at different times: $t = 0$ (*upper left*), $t = 5$ (*upper right*), $t = 10, 15, 20, 25$. The contours give 30%, 50%, 70% and 90% of the maximum velocity in each diagram. The dotted lines correspond to negative velocities, whereas the solid lines give positive velocities. The zero-velocity contour is shown with a dashed line. The equilibrium model is perturbed by an $m = 3$-mode.

Despite the centrifugal balance, the components are not in equilibrium. Mass transformations given by the right-hand-sides of the continuity Eqs. (6)-(8) change the densities and total masses of the components, and the system evolves even without initial perturbations. Fig. 8 illustrates such mass transformation. At the beginning, the mass of the system is contained in the gaseous phase, and by the end of the computation about 90% of the gas has been converted into stellar remnants or long-lived low mass stars. The fraction of mass contained in massive stars drops from the initial value to 0.1% at the end of the simulation.

With the $m = 2$ perturbation given by Eq. (20), all three phases develop a two-armed spiral pattern. Fig. 9 shows the time dependence of the global amplitudes for the $m = 1$,2,3 and 4-armed global modes growing in the stellar component. Again, the $m = 2$ global mode prevails over its competitors, and compared to the purely stellar disk (Fig. 2) it grows about two orders of magnitude faster developing a nonlinear spiral pattern.

Figs. 10 and 11 show the time sequence of the contour plots of the density distributions of the stellar and gaseous components of a disk with an exponential density profile. Initially, the density distribution evolves similarly to the dynamics of the one-component disk, but the subsequent behavior is different. A comparison of Fig. 10 with the simulations in a one-component disk clearly shows that spirals are better developed in a multi-component disk.

A similar behavior was observed for the disk with the Gaussian surface density profile which was seeded by the $m = 3$ perturbation. Fig. 12 shows the growth of the global amplitude in the stellar component of the multi-phase disk accompanied by the mass transformations illustrated on Fig. 13. Again, a comparison with Fig. 5 demonstrates, that the growth rate of the

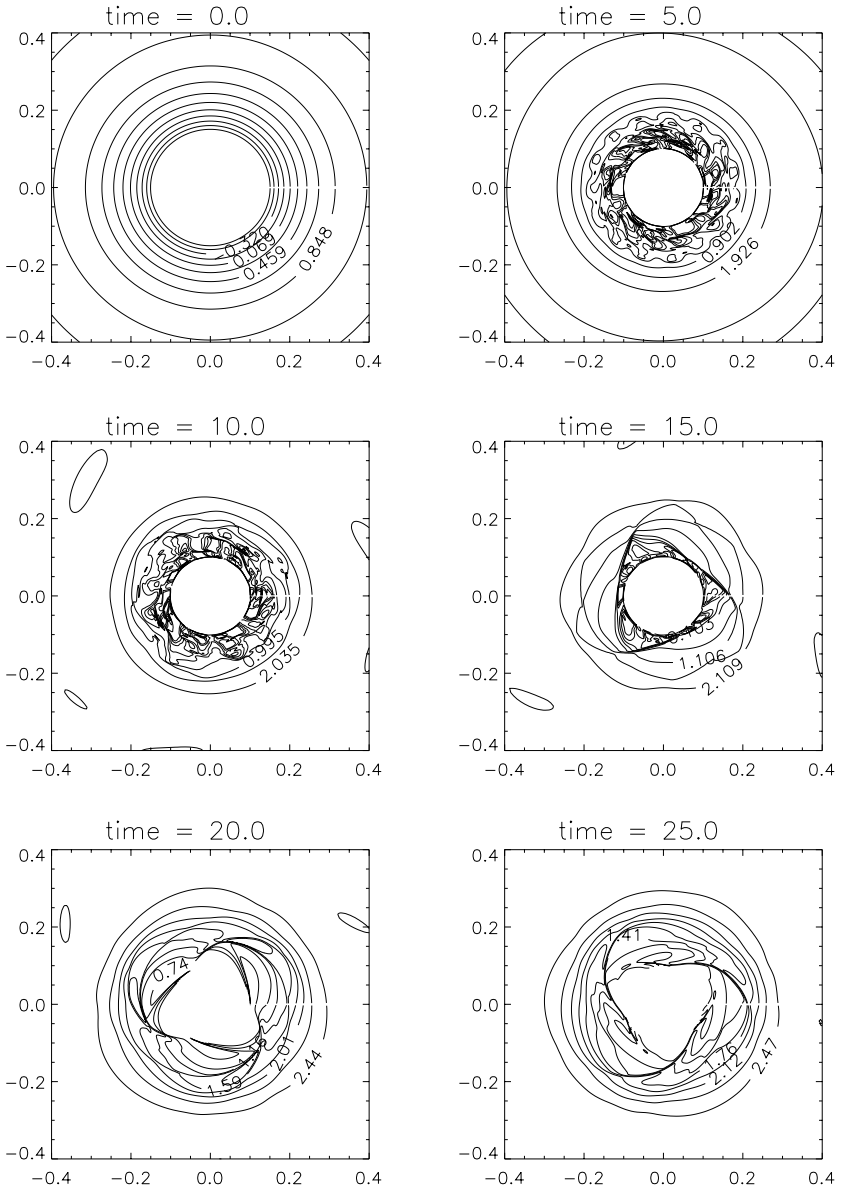


**Fig. 16.** Contour maps of the logarithmic surface density ($\mathrm{M}_\odot/\mathrm{pc}^2$) of the stellar remnant component for the multi-phase Gaussian disk at different times: $t = 0$ (*upper left*), $t = 5$ (*upper right*), $t = 10, 15, 20, 25$. The contours are logarithmic-equally spaced. The equilibrium model is perturbed by an $m = 3$-mode.

$m = 3$ spiral perturbation of the multi-phase disk is an order of magnitude larger than that of the one-component system.

The exponential growth of the $m = 3$ perturbation is changed by the lingering saturation phase occurring at the amplitude level $\log(A_3) \approx -0.1$. This nonlinear saturation of global modes is known for one-component simulations (Laughlin & Różyczka 1996, Laughlin et al. 1997, 1998). Our result shows that the nonlinear saturation of exponentially growing global modes is a common phenomenon which occurs as well in the multi-phase gravitating disks experiencing phase transitions.

The three-armed nature of the perturbations in the multi-component disk is perfectly illustrated in Figs. 14 and 15 which show the contour map of the surface density and the radial velocity of the gaseous phase in a multi-component disk. We note that at late phases of the evolution the gas contains about 8% of the total disk mass, but nevertheless it is still a good tracer of the spiral structure. Moreover, our simulations allow to conclude, that the gas "helps" to develop spiral arms. A comparison of the density distribution of the collisionless remnants phase in a multi-component disk (Fig. 16) with perturbations in a purely stellar disk (Fig. 6) supports this conclusion: The density perturbation in remnants is more organized, and clearly depicts a three-armed spiral.

The destabilizing role of the cold gaseous component was studied for the linear regime by various authors. Local analysis performed by Lin and Shu (1966), Lynden-Bell (1967), Miller et al. (1970), Quirk (1971), Jog & Solomon (1984), Sellwood & Carlberg (1984), and semi-analytical global modal analysis of Bertin & Romeo (1988) demonstrated that a small admixture of gas in a stellar self-gravitating disk may considerably destabilize the system. Our simulations are in agreement with this conclusion, and illustrate, how the spiral structure behaves

on a nonlinear stage. Spiral structure remains well developed and is self-sustained after a rapid star-formation process in a gaseous disk when most of the gas is transformed into a "remnants" phase with higher velocity dispersion, and with a more rigid equation of state.

## 8. Conclusions

In this paper we modeled the generation of spiral structure in a multi-phase, star-forming disk. The gaseous and stellar phases interact as well by their common gravity as by mutual phase transitions due to star formation and stellar death. The main results of our paper can be summarized as follows:

1. The multi-phase disks which undergo a gas–star phase transformations are unstable with respect to nonaxial perturbations. The global spiral modes grow exponentially and saturate in a way, similar to that found in the one-component case.
2. The spiral pattern grows faster and saturates on a higher level compared to a one-component stellar disk with the same mass and rotation. The spiral mode remains well developed, and keeps its properties unaltered if most of the gas is transformed into the "stellar" component with a stiffer equation of state. The cold gas phase remains a good tracer of the spiral structure even if the system contains about a few percent of the total mass of the disk.

These results demonstrate that the destabilizing role of the cold gas component previously known for two-component systems with fixed background properties can be extended to multi-component star-forming disks which are allowed for rapidly changing background properties.

Further research, however, should be performed with respect to self-gravitating multi-component disks. One obvious generalization is necessitated by the simplified model of the interaction chain used in our paper. Interactions between the different phases in a star-forming region are regulated mainly by the time dependent balance between the three components: gas, molecular clouds and stars (e.g. Theis et al. 1992, Shore & Ferrini 1995). Therefore, in a next step the gaseous phase should be split into clouds and an inter-cloud medium matching the chemo-dynamical approach of e.g. Samland et al. (1997). Another aspect is the stochasticity provided by the star-formation in individual clouds. Thus, in extension of Gerola & Seiden's (1978) analysis based on cellular automata, a study of the interplay between large-scale structure formation (including self-gravity) and stochastic processes would be interesting.

*Acknowledgements.* We thank Greg Laughlin for providing his code and for valuable insights into the van Leer advection scheme. We are also grateful to Gerd Hensler for comments and discussions on chemo-dynamical evolution of galaxies. This work was supported by Deutsche Forschungsgemeinschaft with grant 436RUS17/121/96S. VK thanks Prof. Miyama for his kind hospitality at NAO where part of this work was performed.

## Appendix A: parameters for numerical simulations

**Table A1.** Parameters for the exponential disk (cf. Eqs. (16) and (17))

| | |
|---|---|
| General parameters: | |
| Courant factor | $C_f = 0.6$ |
| Bulge mass | $M_B = 0.4$ |
| Bulge scale length | $R_B = 0.4$ |
| Halo mass | $M_H = 1.6$ |
| Halo scale length | $R_H = 0.32$ |
| Inner disk radius | $R_{\rm in} = 0.1$ |
| Outer disk radius | $R_{\rm out} = 1.0$ |
| Mass exchange parameters: | |
| Stellar lifetime | $\tau = 0.075$ |
| Fraction of massive stars | $\zeta = 0.12$ |
| Fraction of mass returned to ISM | $\eta = 0.9$ |
| SFR parameter | $C_2 = 0.1$ |
| Disk (general): | |
| | $d_1 = 1.1$ |
| | $d_2 = 8.0$ |
| | $d_3 = 16.0$ |
| | $r_s = 0.316$ |
| Gaseous disk: | |
| Initial mass | $M_g = 0.22$ |
| Polytropic index | $\gamma_g = 1.67$ |
| Polytropic coefficient | $K_g = 0.005$ |
| Stellar disk: | |
| Initial mass | $M_s = 0.001$ |
| Polytropic index | $\gamma_s = 2.0$ |
| Polytropic coefficient | $K_s = 0.01$ |
| Remnants disk: | |
| Initial mass | $M_r = 0.001$ |
| Polytropic index | $\gamma_r = 2.0$ |
| Polytropic coefficient | $K_r = 0.01$ |

**Table A2.** Parameters for the Gaussian disk (cf. Eqs. (18) and (19))

| | |
|---|---|
| General parameters: | |
| Courant factor | $C_f = 0.5$ |
| Bulge mass | $M_B = 0.15$ |
| Bulge scale length | $R_B = 0.2$ |
| Halo mass | $M_H = 10.0$ |
| Halo scale length | $R_H = 0.25$ |
| Velocity parameter | $v_\infty = 1.5$ |
| Inner disk radius | $R_{\rm in} = 0.1$ |
| Outer disk radius | $R_{\rm out} = 1.0$ |
| Mass exchange parameters: the same | |
| Disk (general): | |
| | $r_s = 0.316$ |
| | $R_0 = 0.45$ |
| | $\omega = 0.05$ |
| Gaseous disk: | |
| Initial mass | $M_g = 0.5$ |
| Polytropic index | $\gamma_g = 1.67$ |
| Polytropic coefficient | $K_g = 0.04$ |

**Table A2.** (continued)

| | |
|---|---|
| Stellar disk: | |
| Initial mass | $M_s = 0.01$ |
| Polytropic index | $\gamma_s = 2.0$ |
| Polytropic coefficient | $K_s = 0.08$ |
| Remnants disk: | |
| Initial mass | $M_r = 0.01$ |
| Polytropic index | $\gamma_r = 2.0$ |
| Polytropic coefficient | $K_r = 0.08$ |

## References


Bertin G., Romeo A.B., 1988, A&A 195, 105

Binney J., Tremaine S., 1987, Galactic Dynamics. Princeton University Press, Princeton

Bottema R., 1993, A&A 275, 16

Gerola H., Seiden P.E., 1978, ApJ 223, 129

Hensler G., Samland M., Theis Ch., Burkert A., 1993, In: Hensler, et al. (eds.) Proc. of Panchromatic View of Galaxies. Kiel, Editions Frontières, p. 342

Jog C.J., Solomon P.M., 1984, ApJ 276, 114

Kato S., 1972, PASJ 24, 61

Kato S., 1974, PASJ 26, 207

Kikuchi N., Korchagin V., Miyama S.M., 1997, ApJ 478, 446

Köppen J., Theis Ch., Hensler G., 1995, A&A 296, 99

Laughlin G., Różyczka M., 1996, ApJ 456, 279

Laughlin G., Korchagin V., Adams F., 1997, ApJ 477, 410

Laughlin G., Korchagin V., Adams F., 1998, ApJ 504, 945

Lin C.C., Shu F., 1966, Proc. Nat. Acad. Sci. USA 55, 229

Lynden-Bell D., 1967, Lect. Appl. Math. 9, 131

Marochnik L.S., 1966, AZh, 43, 919

Miller R.H., Prendergast K.H., Quirk W.J., 1970, ApJ 161, 903

Quirk W.J., 1971, ApJ 167, 7

Samland M., 1994, Ph.D. Thesis, Univ. of Kiel

Samland M., Hensler G., Theis Ch., 1997, ApJ 476, 544

Sellwood J.A., Carlberg R.G., 1984, ApJ 282, 61

Shore S.N., Ferrini F., 1995, Fundam. Cosm. Phys. 16, 1

Stone J.M., Norman M.L., 1992, ApJS 80, 753

Theis Ch., Burkert A., Hensler G., 1992, A&A 265, 465

Vauterin P., Dejonghe H., 1996, A&A 313, 465